Capillarity

Vol. 11, No. 2, p. 41-52, 2024

Original article

Evaluation of immiscible two-phase quasi-static displacement flow in rough fractures using LBM simulation: Effects of roughness and wettability

Xin Zhou[1,2], Jianlong Sheng[1,2], Zuyang Ye[1,2]*

[1]School of Resource and Environmental Engineering, Wuhan University of Science and Technology, Wuhan 430081, P. R. China

[2]Hubei Key Laboratory for Efficient Utilization and Agglomeration of Metallurgic Mineral Resources, Wuhan University of Science and Technology, Wuhan 430081, P. R. China

Keywords:
Rock fractures
two-phase flow
quasi-static displacement
roughness
wettability
LBM simulation

Cited as:
Zhou, X., Sheng, J., Ye, Z. Evaluation of immiscible two-phase quasi-static displacement flow in rough fractures using LBM simulation: Effects of roughness and wettability. Capillarity, 2024, 11(2): 41-52.
https://doi.org/10.46690/capi.2024.05.02

Abstract:
Roughness and wettability of the fracture surface have crucial effects on the two-phase flow properties in many applications involving fractured rock. The immiscible quasi-static displacement flow is widely concerned in porous media, but this phenomenon has been rarely explored in rough-walled fractures. In this study, based on fractal theory and a matched fracture model, three-dimensional fractures with different roughness surfaces and uniform aperture distribution are generated. The lattice Boltzmann-based multicomponent Shan-Chen model is employed to simulate the quasi-static drainage process under various wettability conditions through rough fractures. In fractures with greater roughness and stronger wettability, the displacement process is usually more unstable with more tortuous invasion fronts, which leads to larger entry pressure and displacement resistance. Accordingly, more residual saturation of the wetting phase and lower displacement efficiency occurs under the same capillary pressure. During the invasion process, because of the transverse and delaying development of displacement fronts, the frontmost position is sometimes almost unchanged, while the wetting phase saturation sharply decreases showing a "step-like" type curve. The residual capture patterns are generally divided into two types: "isolated trapping" capture located in areas with drastic undulations of surface, and "water film" capture adsorbed to the fracture surface. Stronger wettability induces more second captures due to the greater adsorption of wetting phase to the fracture wall. A continuous increase in capillary pressure has no apparent effect on the variation in wetting phase saturation when it is greater than the entry pressure, and the first corner on the left side of capillary pressure-wetting phase saturation curves is relatively sharp.

1. Introduction

Immiscible two-phase displacement flow in rock fractures is a widely applied phenomenon in many practical projects, such as CO_2 geological storage, oil and gas extraction, geothermal energy development, or polluted groundwater remediation (Chang et al., 2020; Yao et al., 2020; Al-Hashimi et al., 2021; Ye et al., 2021, 2023). Influenced by many factors including the fluid properties of two immiscible fluids (interfacial tension, viscosity, density), flow conditions, fracture geometry (roughness, aperture distribution), wettability, and so on, the two-phase displacement process in porous and fractured media often presents various displacement patterns and complex flow structures at the microscale, further leading to many elusive macroscopic properties such as invasion pattern, entry pressure, displacement efficiency, and residual capture (Chen et al., 2017, 2018; Wang and Cardenas, 2018; Sheng et al., 2019; Cai et al., 2022; Liu et al., 2022; Wang et al., 2023). Therefore, investigating the two-phase displacement

*Corresponding author.
E-mail address: zhouxin_wust@163.com (X. Zhou); wkdsjl@163.com (J. Sheng); yezuyang@wust.edu.cn (Z. Ye).

Yandy Scientific Press

Received January 7, 2024; revised January 28, 2024; accepted February 17, 2024; available online February 21, 2024.

flow behavior and its intrinsic mechanism in rough-walled fractures has been a significant scientific challenge that needs to be urgently addressed.

Fracture geometry and wettability are two crucial factors affecting the two-phase flow characteristics, which have attracted extensive research attention. As an important form of two-phase flow, immiscible two-phase displacement flow was firstly described in a pioneer study of porous media (Lenormand et al., 1988). Therein, the invading phase was injected into a two-dimensional porous medium to displace the defending phase and high-resistance regions were usually bypassed with the formation of many residual captures. Subsequently, the effect of geometric characteristics on the displacement process and specific appearance was further investigated within fractured media through many experimental studies, which suggested that the invasion front, flow paths and capture patterns are closely related to the spatial distribution of aperture and surface morphology of the fracture (Neuweiler et al., 2004; Karpyn et al., 2007; Al-Housseiny et al., 2012; Babadagli et al., 2015a, 2015b). A quantitative investigation of surface roughness effects was performed by Hu et al. (2019), which involved water-oil invasion tests in a transparent rough-walled fracture. They found that the increase in relative roughness resulted in more unstable displacement front and higher energy dissipation. In addition to laboratory tests, numerical simulation is an effective alternative to explore the two-phase displacement flow phenomenon in rough fractures. Pruess et al. (1990) developed a percolation method for two-phase flow in variable-aperture fractures based on the assumption of two-dimensional porous media and the local parallel-plate model, and demonstrated that residual saturations and relative permeabilities were strongly influenced by the spatial correlation of fracture apertures due to the strong two-phase interference. A similar invasion percolation method that focuses on two-phase displacement flow through horizontal fractures was employed in numerous other researches (Glass et al., 1998; Ye et al., 2015, 2017; Wang and Cardenas, 2018; Yang et al., 2019). Although the effects of fracture geometry, including roughness, spatial distribution and correlation length of aperture, on the displacement flow properties were deeply explored in these experimental and simulation studies, the wettability of fracture wall was rarely considered, which plays an important role in two-phase displacement flow processes.

Thus far, the impact of wettability on two-phase displacement flow has been studied in porous media extensively through visualized two-phase invasion experiments in two-dimensional microfluidic models (Holtzman and Segre, 2015; Trojer et al., 2015; Zhao et al., 2016). It was demonstrated that the change in wall wettability alters the fluid-wall contact features, which significantly affects the two-phase flow patterns and the displacement efficiency. However, due to the difficulty of controlling the wettability of rough-fracture wall, experimental studies on the wettability of two-phase displacement flow in fractured media have been scarce. Bergslien and Fountain (2006) performed hydrophobic and hydrophilic treatments to transparent fracture surfaces using polystyrene coating and low-temperature plasma, respectively, where the invading fluid was more likely to form connected channels in hydrophobic fractures, while in hydrophilic fractures, it was limited to larger pore size areas without a stable flow path. Babadagli et al. (2015a, 2015b) executed a series of water-gas and water-oil displacement experiments, which indicated that in addition to roughness, the wettability of fractures with various rock lithology is a critical factor affecting the residual and initial saturations, especially for liquid-liquid systems. Recently, Qiu et al. (2023) conducted water-oil displacement experiments in a rough micro-fracture model and found that wettability alteration caused by various forms of water film on fracture surfaces with different roughness produces diverse displacement patterns and residual distributions. However, these experiments only involved preliminary studies on the influence of wettability during the displacement flow process, while the relationship between two-phase displacement properties and wettability in fractures, especially for those in quasi-static state, still needs further investigation.

Compared to displacement flow experiments, numerical simulation can better study the effect of wettability in rough fractures on two-phase displacement flow. Due to its flexibility in complex media and high computational performance, the lattice Boltzmann method (LBM), as a mesoscopic numerical method, has been developed over the past three decades to simulate single-phase flow (Chaaban et al., 2020; Ma et al., 2022) and multiphase flow (Wang et al., 2019; Cao et al., 2020). Researchers have adopted LBM multiphase models to control the fluid wettability through simulating the variations in contact angle between wall and fluids and have achieved fruitful results for porous media (Landry et al., 2014; Zhao et al., 2018; Guo et al., 2022). Nonetheless, multiphase flow paths through pores differ from those in fractures due to the irregular geometric structures found in nature; furthermore, studies on the influence of wettability in fractured media on the displacement flow have been relatively infrequent. Dou et al. (2013) investigated the effect of wettability on the drainage process in self-affine rough fractures through LBM simulations, which revealed that stronger wettability produces the growth of capillary pressure, interfacial area and irreducible water saturation. Guiltinan et al. (2021) considered the influence of heterogeneous wettability and fracture geometry, including mean aperture and roughness, on the scCO_2-water dynamic displacement process and found that the wettability distribution is closely related to the residual capture of water saturation. Yi et al. (2021) investigated the effect of wettability on the two-phase flow characteristics in two-dimensional rough fractures using LBM. The results showed that wettability affected the distribution of micro-scale flow and the relative permeability of fracture. Meanwhile, these studies overlooked the influences of fracture roughness on quasi-static displacement in three-dimensional rough fractures.

Consequently, it is worthwhile to assess the combined effects of fracture roughness and wettability on quasi-static displacement flow in rough rock fractures. Specifically, it is also required to elucidate the displacement flow properties including saturation evolution, residual capture and capillary pressure-saturation relationship of quasi-static invasion in fractures with different geometrical characteristics. To address these problems, the present study generated three-dimensional

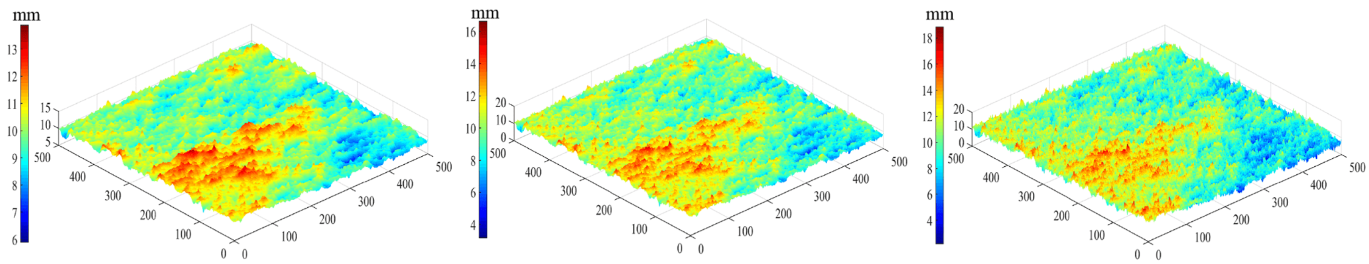

(a) $D = 2.1$ (b) $D = 2.3$ (c) $D = 2.5$

Fig. 1. Comparison of surface morphology of rough fractures with various fractal dimensions (red represents greater height, and blue represents smaller height, unit: mm).

rough-fracture surfaces based on fractal theory and established fracture models with various roughness through duplication and translation operations. Then, the quasi-static drainage process under different wettability conditions in rough fractures was simulated by the LBM multicomponent Shan-Chen model, and accordingly, the influence of fracture roughness and wettability on two-phase displacement flow properties and corresponding microscopic mechanism were elaborately explored.

2. Numerical methods

2.1 Fractal rough-walled fractures

The rough surfaces of natural rock fracture basically satisfy self-affine fractal distribution (Brown, 1987; Charkaluk et al., 1998), which is commonly modeled by fractional Brownian motion. The height of these surfaces can be described by a random, continuous and single-valued function $Z(x)$. The stationary increment of height $[Z(x) - Z(x+\lambda\Delta)]$ over the distance Δ follows Gaussian distribution with mean zero and variance δ^2:

$$\langle Z(x) - Z(x+\lambda\Delta) \rangle = 0 \tag{1}$$

$$\delta_{\lambda\Delta}^2 = \left\langle [Z(x) - Z(x+\lambda\Delta)]^2 \right\rangle \tag{2}$$

$$\delta_{\Delta}^2 = \left\langle [Z(x) - Z(x+\Delta)]^2 \right\rangle \tag{3}$$

where $\langle\cdot\rangle$ represents the mathematical expectation, x denotes the coordinate component, λ is a constant, $\delta_{\lambda\Delta}^2$ and δ_{Δ}^2 are the variances corresponding to height variation with the distance of $\lambda\Delta$ and Δ, respectively. The self-affinity relating to fractional Brownian motion obeys the following expressions:

$$\left\langle [Z(x) - Z(x+\lambda\Delta)]^2 \right\rangle = \lambda^{2H} \left\langle [Z(x) - Z(x+\Delta)]^2 \right\rangle \tag{4}$$

Hence, combining Eqs. (2) and (3), Eq. (4) can be rewritten as:

$$\delta_{\lambda\Delta}^2 = \lambda^{2H} \delta_{\Delta}^2 \Rightarrow \delta_{\lambda\Delta} = \lambda^H \delta_{\Delta} \tag{5}$$

where H represents the Hurst exponent that varies from 0 to 1, which is associated with the fractal dimension by $D = 3 - H$ for two-dimensional surface. In the present study, the successive random addition method (Liu et al., 2004; Ye et al., 2015, 2017) is adopted to generate rough-walled fracture surfaces. According to previous research results, the fractal dimension D of natural rough fractures is set between 2.0 and 2.6 (Brown, 1987). The generated fracture surfaces with various fractal dimensions are shown in Fig. 1. The side length L of square is equal to 500 mm, and fractal dimensions D of 2.1, 2.3 and 2.5 are selected. It can be seen that with the increase in D, which means greater roughness, the fracture surface shows a wider range of elevation change with increasing maximum and decreasing minimum values of height, and the elevations of adjacent points are more scattered and fluctuating.

2.2 Multicomponent Shan-Chen model

The multicomponent Shan-Chen (MCSC) model (Shan and Chen, 1993), which is one of the most prevalent and commonly used LBM models for immiscible multiphase flow, is employed in this study to simulate two-phase displacement processes through rough fractures. In the MCSC model, the distribution probability of microscopic particle clusters for immiscible two-phase fluids are represented by two groups of particle distribution functions $f_i^{\alpha}(x,t)$, in which $\alpha = w, n$ denotes wetting phase and non-wetting phase, respectively. Introducing the single-relaxation-time Bhatnagar-Gross-Krook operator, the evolutions of particle distribution function $f_i^{\alpha}(x,t)$ for each fluid satisfies the discretized form of continuous Boltzmann equation:

$$f_i^{\alpha}(x,t) - f_i^{\alpha}(x + c_i\Delta t, t + \Delta t) = \frac{\Delta t}{\tau^{\alpha}} \left[f_i^{\alpha}(x,t) - f_i^{\alpha(eq)}(x,t) \right] \tag{6}$$

where the subscript i represents the direction of associated discrete velocity, and $f_i^{\alpha}(x,t)$ represents the particle distribution function of α component with ith discrete velocity c_i at position x and time t. The parameter τ^{α} denotes the relaxation time of α component, which determines the average time interval of the equilibrium process and is related to the kinematic viscosity of fluids $v = c_s^2(\tau - 1/2)$, where $c_s = c/\sqrt{3}$ denotes the speed of sound of the lattice. The equilibrium distribution function $f_i^{\alpha(eq)}(x,t)$ is defined as:

$$f_i^{\alpha(eq)}(x,t) = w_i \rho^{\alpha} \left[1 + \frac{u \cdot c_i}{c_s^2} + \frac{(u \cdot c_i)^2}{2c_s^4} - \frac{u^2}{2c_s^2} \right] \tag{7}$$

$$[c_0,c_1,c_2,c_3,c_4,c_5,c_6,c_7,c_8,c_9,c_{10},c_{11},c_{12},c_{13},c_{14},c_{15},c_{16},c_{17},c_{18}] = c\begin{bmatrix} 0 & -1 & 1 & 0 & 0 & 0 & 0 & 1 & -1 & 0 & 0 & -1 & 1 & -1 & 1 & 0 & 0 & 1 & -1 \\ 0 & 0 & 0 & -1 & 1 & 0 & 0 & 1 & -1 & -1 & 1 & 0 & 0 & 1 & -1 & 1 & -1 & 0 & 0 \\ 0 & 0 & 0 & 0 & 0 & 1 & -1 & 0 & 0 & 1 & -1 & 1 & -1 & 0 & 0 & 1 & -1 & 1 & -1 \end{bmatrix} \tag{8}$$

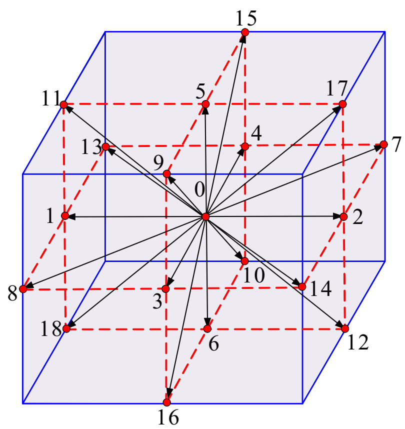

Fig. 2. Illustration of the D3Q19 LBM model.

where $u = u^{\alpha(eq)}$ and ρ^{α} represent the macroscopic velocity and density of the α component, respectively; w_i denotes the weight for specific velocity set. Here, we choose the D3Q19 model as illustrated in Fig. 2, in which the particle distribution function has 19 discrete velocities including a zero velocity and 18 velocities communicating with neighboring lattice nodes, and the corresponding weights are $w_i = 1/3$ $(i = 0)$, $w_i = 1/18$ $(i = 1 \sim 6)$, $w_i = 1/36$ $(i = 7 \sim 18)$, respectively. For the simplicity of computation, the lattice spacing Δx and time step Δt are set to one, thus the lattice speeds $c_i = [c_{ix}, c_{iy}, c_{iz}]$, which are defined as the ratio of Δx to Δt, are given by Eq. (8).

After the streaming step according to the left side of Eq. (6), the macroscopic density and velocity of fluids can be calculated by:

$$\rho^{\alpha} = \sum_i f_i^{\alpha} \tag{9}$$

$$u^{\alpha} = \frac{\sum_i f_i^{\alpha} c_i}{\sum_i f_i^{\alpha}} \tag{10}$$

The common averaged velocity u' of two components is given by:

$$u' = \frac{\dfrac{\sum_{\alpha} \rho^{\alpha} u^{\alpha}}{\tau^{\alpha}}}{\dfrac{\sum_{\alpha} \rho^{\alpha}}{\tau^{\alpha}}} \tag{11}$$

In the MCSC model, the fluid-fluid interaction is provided by a pseudopotential cohesive force $F_c^{\alpha}(x,t)$ acting on fluid particles, defined as:

$$F_c^{\alpha}(x,t) = -G_c \rho^{\alpha}(x,t) \sum_i w_i \rho^{\bar{\alpha}} (x + c_i \Delta t, t) c_i \tag{12}$$

where α and $\bar{\alpha}$ represent two different fluid components, and G_c is a parameter that controls the cohesive strength between two fluids. The adhesive force $F_s^{\alpha}(x,t)$ acting between fluid particles and solid wall for the α component can be calculated by:

$$F_s^{\alpha}(x,t) = -G_s^{\alpha} \rho^{\alpha}(x,t) \sum_i w_i s(x + c_i \Delta t, t) c_i \tag{13}$$

where $s(x + c_{\alpha} \Delta t, t)$ is an indicator function that equals zero for a fluid node and one for a solid node in the computational domain. G_s^{α} is a parameter to adjust the adhesive strength between fluids and solid wall and to change the wettability for the α component. For the absence of any external force, the total force $F^{\alpha} = F_c^{\alpha} + F_s^{\alpha}$ acting on α component provides acceleration into the velocity field, therefore the macroscopic equilibrium velocity of α component is given by:

$$u^{\alpha(eq)} = u' + \frac{\tau^{\alpha} F^{\alpha}}{\rho^{\alpha}} \tag{14}$$

The equilibrium distribution function $f_i^{\alpha}(x,t)$ can be determined through Eq. (7) when $u^{\alpha(eq)}$ is known, and then the collision step is completed based on the right side of Eq. (6). The above steps are repeated until the simulation has converged, and the pressure P and mixed fluid velocity at lattice nodes for each iteration can be obtained by:

$$P = c_s^2 \sum_{\alpha} \rho^{\alpha} + \frac{G_c}{3} \rho^{\alpha} \rho^{\bar{\alpha}} \tag{15}$$

$$v = u' + \frac{\sum_{\alpha} F^{\alpha}}{2 \sum_{\alpha} \rho^{\alpha}} \tag{16}$$

In the present work, all simulations for two-phase flow were carried out using the LBM open-source code Palabos version 2.2 (Latt et al., 2021; Santos et al., 2022) on Linux platform.

2.3 Contact angle verification

The wettability of fracture surface is characterized directly by the contact angle, thus it is worth verifying the effectiveness of the MCSC model in simulating various contact angles to ensure the reliability of research results for the wettability effect. According to Yang's equation, wettability is related to the energy parameters of fluid-fluid and fluid-solid interactions (Shan et al., 2022); an approach to determine the contact angle was proposed by Huang et al. (2007):

$$\cos\theta = \frac{2(G_{s,1} - G_{s,2})}{G_c(\rho_1 - \rho_2)} \tag{17}$$

where $G_{s,1}$, $G_{s,2}$ represent the adhesive strength parameter of wetting phase and non-wetting phase, respectively, which are set to $G_{s,2} = -G_{s,1}$ as suggested in previous literatures (Huang et al., 2007; Landry et al., 2014); ρ_1 and ρ_2 are the dominant

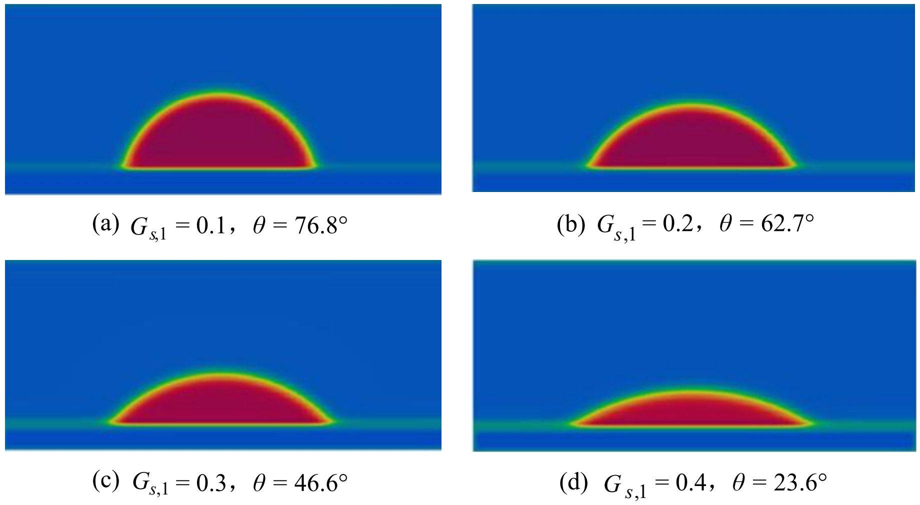

Fig. 3. Simulation results of contact angle.

Table 1. Parameters of fracture geometry and simulation settings.

Fracture type	Matched rough fractures
Contact angle	23.6°, 46.6°, 62.7°, 76.8°
Adhesive strength	0.4, 0.3, 0.2, 0.1
Model size	$201\times201\times50$ Lu^3
Fractal dimension	2.1, 2.3, 2.5
Mean aperture	10 Lu
Surface tension	0.15
Dissolved density	0.06
Dominant density	2
Kinematic viscosity	0.1667
Relaxation time	1
Cohesive strength	0.9

and dissolved density, respectively. The values of these parameters and other simulation settings used in this study are illustrated in Table 1. Since we mainly focus on the drainage process, the contact angle θ of wetting phase is controlled between 0° and 90°, as shown in Fig. 3. It can be seen that the simulation results of contact angle are reasonably consistent with the predictive values, which indicates that the wettability of the fracture surface is stronger with a smaller contact angle as the value of $G_{s,1}$ increases. For simplicity, different wettability is identified by the theoretical values of contact angle in subsequent analysis.

2.4 Computational settings

In order to quantify the effect of fracture surface roughness on the two-phase displacement flow properties, the generated fracture surfaces with diverse surface roughness in Fig. 1 were duplicated and translated upwards by 10 Lu (lattice unit) to construct matched fractures models. In other words, because the main objective is to explore the effects of surface roughness and wettability, the fracture models in the present study process uniform aperture distribution and the same morphology of the upper and lower surfaces with fractal dimension $D=2.1, 2.3, 2.5$. For the purpose of saving computing resources, the final fracture domain is selected as the center 201×201 Lu^2 region from the original fracture model, and the height along the z direction of the computational model is maintained at 50 Lu. Four different wettability conditions of the fracture surface, as shown in Fig. 3, are considered in this study through adjusting the adhesive strength parameter $G_{s,1}$ listed in Table 1, in which the parameters of fracture geometry and simulation settings are also given.

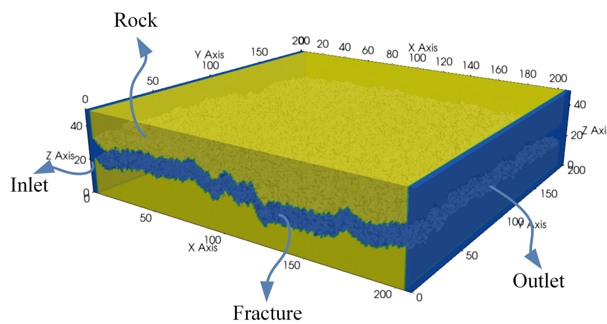

Fig. 4. LBM computational model of a three-dimensional rough fracture with $D=2.3$.

The LBM computational models of matched rough-fracture are constructed by the ternary-processing method. As shown in Fig. 4, the upper and lower parts indicated by yellow color represent the rock matrix with no-dynamic flow conditions, while the blue part in the middle of the computational model represents the flowable region, and 4 Lu layers on both inlet and outlet boundary are reserved at two ends of the fracture to reduce numerical fluctuations. The fracture walls that connect the rock matrix and the fracture domain and two laterals are

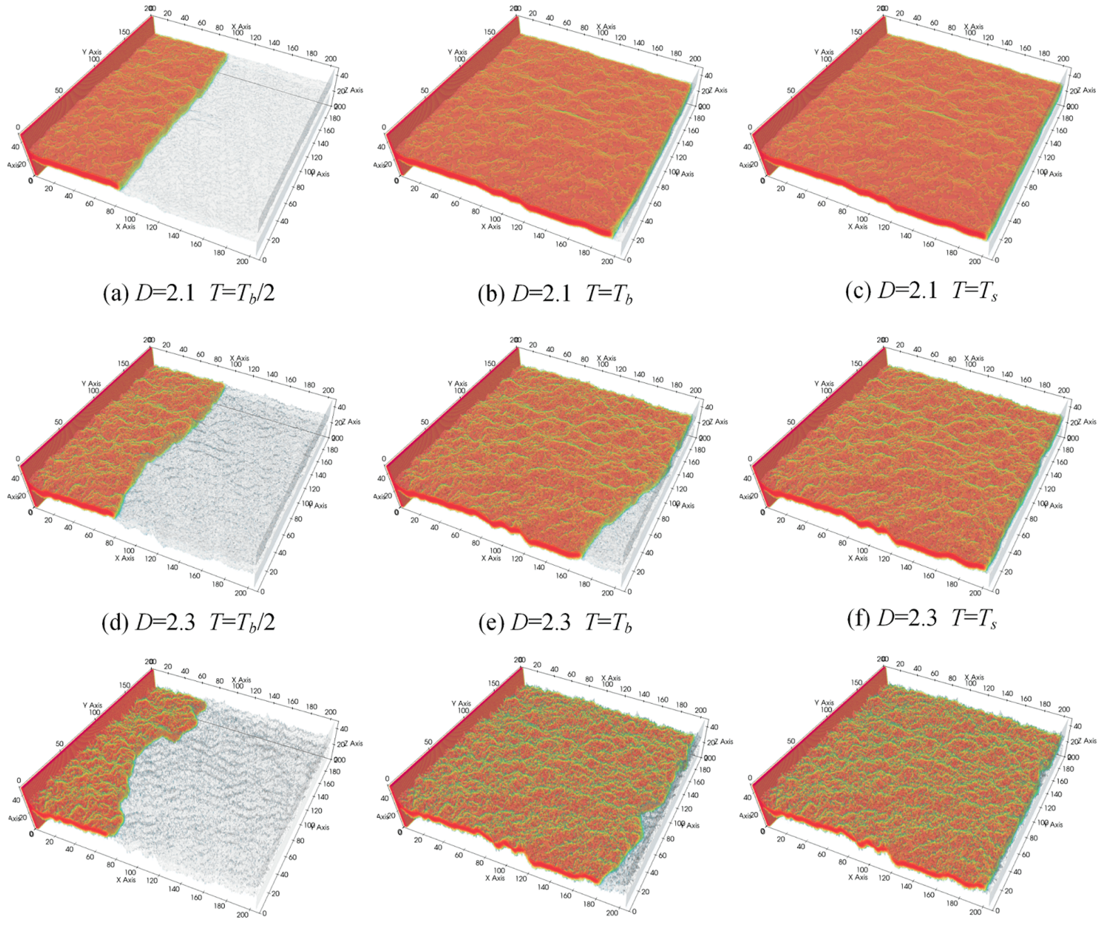

(a) D=2.1 T=T_b/2 (b) D=2.1 T=T_b (c) D=2.1 T=T_s

(d) D=2.3 T=T_b/2 (e) D=2.3 T=T_b (f) D=2.3 T=T_s

(g) D=2.5 T=T_b/2 (h) D=2.5 T=T_b (i) D=2.5 T=T_s

Fig. 5. Displacement process in rough fractures with different roughness for θ = 76.8°.

ascribed the no-slip boundary condition accomplished by the bounce-back scheme. The fracture space is initially saturated with wetting phase and then invaded by non-wetting phase. The pressure boundary conditions are employed on the inlet and outlet of the fracture model (Zou and He, 1997), and the capillary pressure is determined by the difference between the two pressures, where the pressure on the inlet reservoir is kept constant and is decreased gradually on the outlet to achieve the slowly increasing capillary pressure of quasi-steady drainage process (Dou et al., 2013; Yamabe et al., 2015). In other words, when the given smaller pressure difference is not sufficient to drive the wetting phase by a non-wetting phase, the displacement pressure difference is gradually increased for a continuously invading wetting phase in fractures with larger resistance until the displacement process reaches a completely stable state. The capillary number C_a is always below 5×10^{-4}, which means that the viscous force is negligible compared to capillary force. Note that the capillary pressure applied under various wettability conditions is set to distinct values to better adapt to the changing displacement resistance. Because of the effect of gravitation, density and viscosity ratio are not considered here, and the densities and viscosity of wetting phase and non-wetting phase are set as identical values to avoid numerical instability problems (Hao and Cheng, 2010; Tang et al., 2019). It is assumed that if the relative difference of average density over each iteration for both two components is less than 1×10^{-4}, one simulation of drainage process has converged. For simplicity, all variables are measured in lattice units. A total of 12 simulations for three fractures with four wettabilities took about 25 days to run on an Intel CPU i7-12700F desktop computer.

3. Results and discussion

3.1 Two-phase displacement process

During the quasi-static displacement process, the evolution of phase distributions in rough fractures with diverse roughness, including fractal dimensions $D = 2.1, 2.3, 2.5$ for wetting conditions $\theta = 76.8°$ and 23.6°, are given in Figs. 5 and 6, respectively. The orange area represents the non-wetting phase, the remaining part (not colored for easier observation) is the wetting phase, and the grey color denotes the fracture wall. Three typical drainage processes at various moments, including half of the breakthrough time T_b/2, breakthrough time T_b and steady state T_s, are illustrated. It can be seen that surface roughness and wettability have a significant impact on

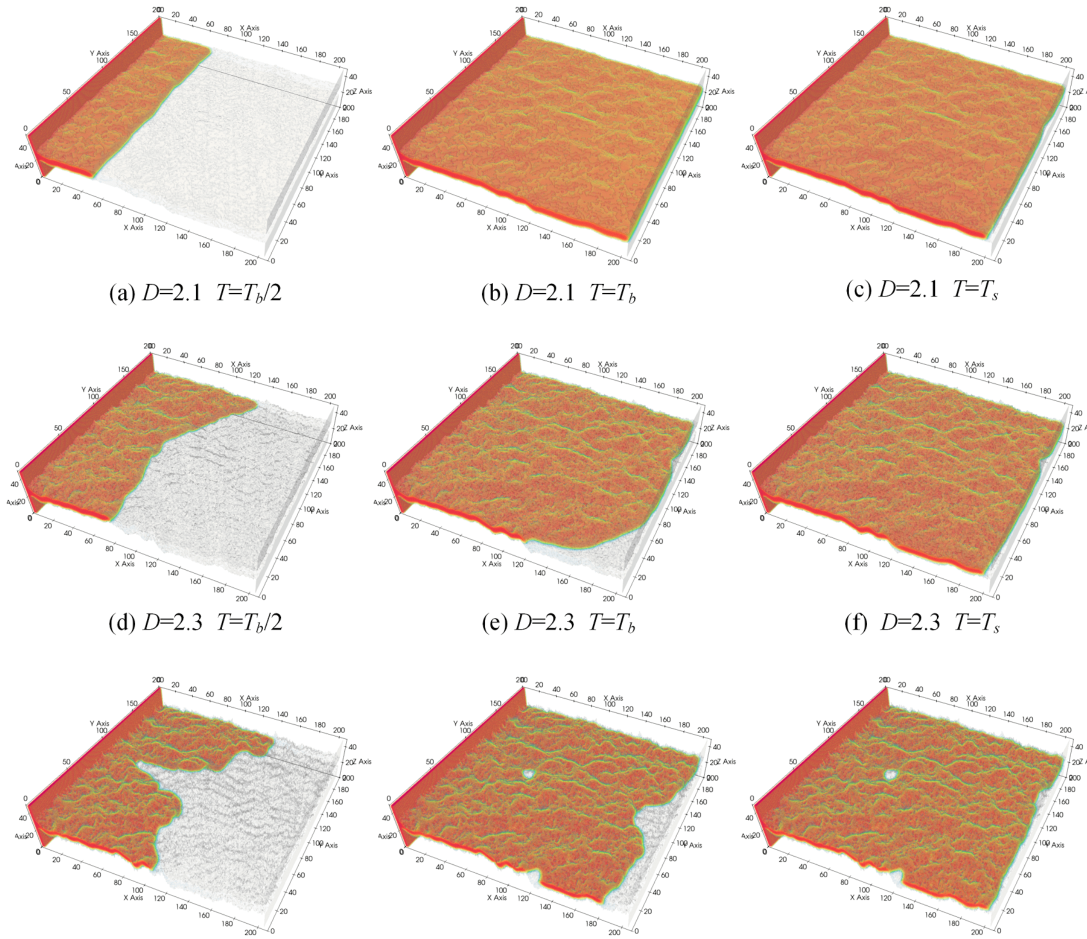

(a) D=2.1 T=T_b/2 (b) D=2.1 T=T_b (c) D=2.1 T=T_s

(d) D=2.3 T=T_b/2 (e) D=2.3 T=T_b (f) D=2.3 T=T_s

(g) D=2.5 T=T_b/2 (h) D=2.5 T=T_b (i) D=2.5 T=T_s

Fig. 6. Displacement process in rough fractures with different roughness for θ = 23.6°.

the two-phase displacement process. The displacement front in the fracture with $D = 2.1$ is very smooth and flat, i.e., close to a straight line (see in Figs. 5(a) and 6(a)), while that in fractures with increasing surface roughness becomes more tortuous and curved during the invasion process. Accordingly, there is a more visible remaining wetting phase near the outlet of fracture that has rougher surface at the breakthrough time (see in Figs. 5(e), 5(h), 6(e) and 6(h)).

On account of the effect of wettability, the appearance of tortuous flow front in fractures with the same morphology for $\theta = 23.6°$ (see in Figs. 6(d) and 6(g)) is more prominent than that for $\theta = 76.8°$ (see in Figs. 5(d) and 5(g)), with the formation of an uneven phase interface in the fracture with $D = 2.5$ (see in Fig. 6(g)). In other words, stronger wettability makes the displacement process generally more unstable and the invasion front more tortuous and irregular. Specifically, due to the combined impacts of wettability and roughness, a region of wetting phase emerges that is very difficult to be intruded, leading to the occurrence of isolated wetting-phase areas trapped by a surrounding non-wetting phase in the fracture with $D = 2.5$ for $\theta = 23.6°$ (see in Figs. 6(h) and 6(i)). Nevertheless, the wetting phases in all fractures for $\theta = 76.8°$ and in smoother fractures for $\theta = 23.6°$ are almost driven at steady state with no clear trapping capture regions. This indicates that fractures with greater roughness and stronger wettability have a larger displacement resistance and more complex flow patterns during the displacement process.

3.2 Saturation distributions

The evolution of wetting phase saturation S_w with the frontmost position of displacement front is illustrated in Fig. 7, where S_w shows a gradually decreasing trend with the advancement of invading front. When the flowing front approaches the fracture outlet, i.e., at breakthrough time, the frontmost position of displacement front no longer increases, while S_w continues to decrease to the residual saturation with the appearance of a vertical downward trend until the displacement flow reaches a steady state. The value of S_w for the same wettability condition becomes larger as the fractal dimension of fracture increases, which indicates that the greater fracture surface roughness causes more capture of the wetting phase at the same frontmost position. As the wettability of fracture surface becomes stronger, the distinct evolution of wetting saturation between fractures with different

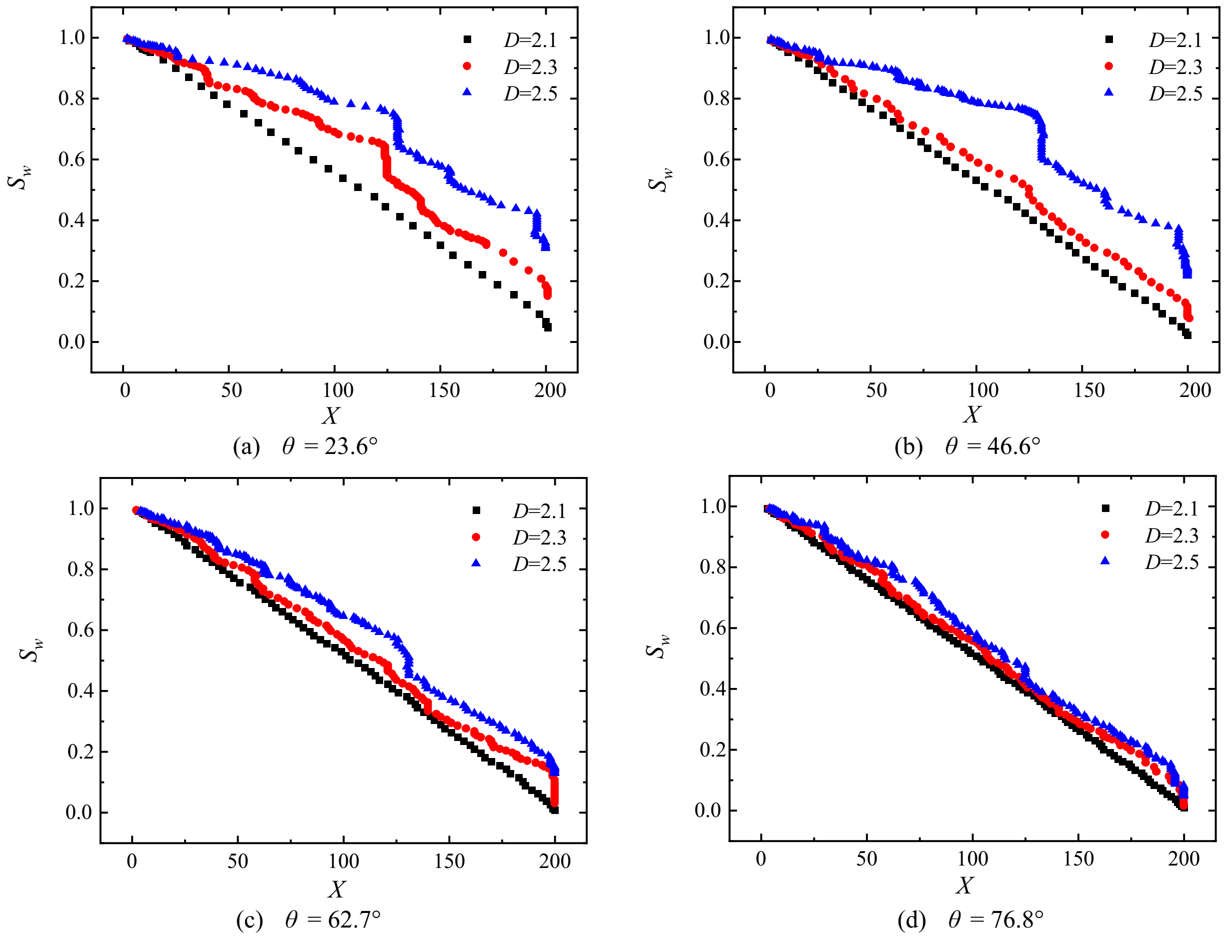

Fig. 7. Relationship between saturation distributions of wetting phase and frontmost position.

roughness gradually increase, showing more relatively discrete S_w-X curves, which means that the enhanced wettability results in the more complicated invasion process is in accordance with the observations of flow patterns in Section. 3.1. Note the presence of a phenomenon that the frontmost position of displacement front is almost unchanged while S_w sharply decreases before breakthrough time, showing a "step-like" type of S_w-X curves. This is because in the invasion process, the frontmost displacement position not only advances forward along the direction parallel to the x-axis but also sometimes develops transversely and does not advance further until it joins other interfaces, as reported in previous researches involving displacement experiments (Chen et al., 2017; Hu et al., 2019).

In order to further quantify the effect of roughness and wettability of the fracture surface on displacement flow processes, the S_w at two important moments, including breakthrough time T_b and steady state T_s, under various wettability conditions are given in Table 2, in which the saturation variation ΔS_w of the wetting phase between T_b and Ts corresponds to the extent of vertical decline of S_w-X curves in Fig. 7. When the fracture surface roughness increases, resulting in more curved flow paths and a slightly more trapping capture (see in Fig. 6), the remaining saturation at T_b and ultimate residual saturation at Ts correspondingly become greater (see in Table 2). The S_w at the two moments (T_b and T_s) generally increase with the growth of wettability, which is more obvious in fractures with greater roughness, such as those with $D = 2.5$ (see in Table 2). Importantly, although apparent "isolated trapping" capture does not occur visibly at the steady state, such as at $D = 2.3$ (see in Figs. 5 and 6), the residual saturation of wetting phase increases with stronger wettability by up to 15% (see in Table 2), suggesting that in addition to the evident "isolated trapping" pattern, there is an undiscovered capture pattern that needs to be further explored.

3.3 Residual capture patterns

For the sake of a deeper exploration of residual capture patterns during the displacement process, Fig. 8 takes the invasion presentation in a fracture with $D = 2.5$ for $\theta = 23.6°$ at steady state as an example, and the cross-section at $X = 64$ is extracted to show the local distribution characteristics of two phases. The two blue curves in cross-section represent the upper and lower rough-walls of fracture, the dark red part in the middle represents the non-wetting phase, and the rest of light-colored region is the wetting phase. It can be seen that the residual wetting phases mainly have two capture patterns in the rough fracture. The first one is the black circled part

Table 2. Wetting phase saturation at breakthrough time and steady state.

Fractal dimension	Condition	Wetting phase saturation (S_w)			
		76.8°	62.7°	46.6°	23.6°
2.1	Breakthrough time T_b	0.021	0.027	0.032	0.066
	Steady state T_s	0.009	0.008	0.022	0.047
	Variation ΔS_w	0.012	0.019	0.010	0.019
2.3	Breakthrough time T_b	0.068	0.141	0.128	0.184
	Steady state T_s	0.014	0.030	0.077	0.150
	Variation ΔS_w	0.054	0.111	0.051	0.034
2.5	Breakthrough time T_b	0.081	0.165	0.305	0.340
	Steady state T_s	0.047	0.129	0.216	0.306
	Variation ΔS_w	0.034	0.036	0.089	0.034

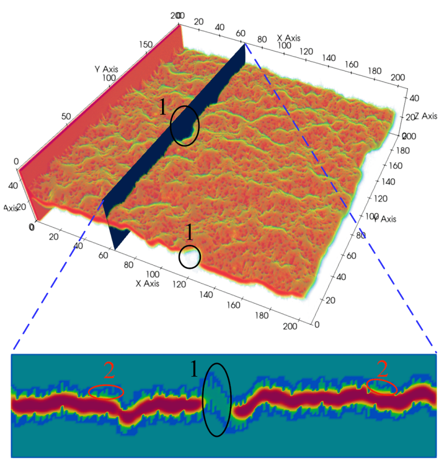

Fig. 8. Illustration of two kinds of residual capture pattern.

(marked as number 1), which is located in areas with drastic undulations of fracture surface. The non-wetting phases bypass this part of the wetting phase, forming an "isolated trapping" capture region, which only occurs in a fracture with $D = 2.5$ for $\theta = 23.6°$ due to the uneven phase interface, as shown in Figs. 5 and 6. The second capture pattern is the part marked by red circle (labeled as number 2), where the wetting phase consistently adsorbs to the rough wall of the fracture and is difficult to be displaced, appearing as a layer of wetting phase like a "water film". As discussed above, the first capture pattern is scarce in the fracture with $D = 2.3$ at steady state, hence the improved saturation of wetting phase with increasing wettability (see in Table 2) mostly comes from the second capture pattern because stronger wettability leads to greater adsorption of wetting phase to the fracture wall, consistent with previous data (Dou et al., 2013; Guiltinan et al., 2021). In addition, the phenomenon of "water film" capture has been widely studied at the micro scale through LBM simulations of porous media. Zhang et al. (2021) found that a water film reduces the pore size for effective gas flow, leading to greater displacement resistance during the gas flow process. Other research results have fully demonstrated that the water film phenomenon is common in two-phase displacement processes and has an important impact on the displacement flow characteristics (Li et al., 2017; Meng and Cai, 2018; Liu et al., 2020; Zhou et al., 2023).

3.4 Relationship of P_c-S_w

The relationship between capillary pressure Pc and wetting phase saturation S_w is presented in Fig. 9, where P_c is expressed in lattice unit for convenience. At the beginning of displacement flow, S_w basically remains unchanged since the small P_c applied at two ends of a fracture is insufficient to overcome the strong capillary resistance. However, when P_c is gradually increased to reach the entry pressure, which is the minimum pressure required for wetting phase to be displaced by non-wetting phase, S_w decreases rapidly and most of the wetting phases are completely expelled due to uniform aperture distribution, except for "water film" capture that is persistently adsorbed on the fracture wall. Therefore, continuously increasing P_c has no apparent effect on S_w variation once P_c is greater than the entry pressure, and the first corner on the left side of P_c-S_w curves is relatively sharp.

The entry pressure P_e is strongly influenced by fracture roughness and wettability. In specific, P_e increases with the improvement of fractal dimension under the same wettability condition, which demonstrates that fractures with greater surface roughness have larger displacement resistance. As a result, the displacement efficiency is lower, i.e., S_w is larger in fractures with greater fractal dimension when the same P_c is applied (see in Fig. 9). On the other hand, for the same fracture, P_e is distinctly enhanced by stronger wettability because of a greater adsorption of wetting phase on the fracture wall, which results in larger capillary resistance in the invasion process. Consequently, stronger wettability leads to more residual wetting phase saturation (see in Table 2) and lower displacement efficiency in the same fracture due to more "isolated trapping" and "water film" captures.

4. Conclusions

In the present work, we investigated the influence of fracture roughness and wettability on immiscible two-phase

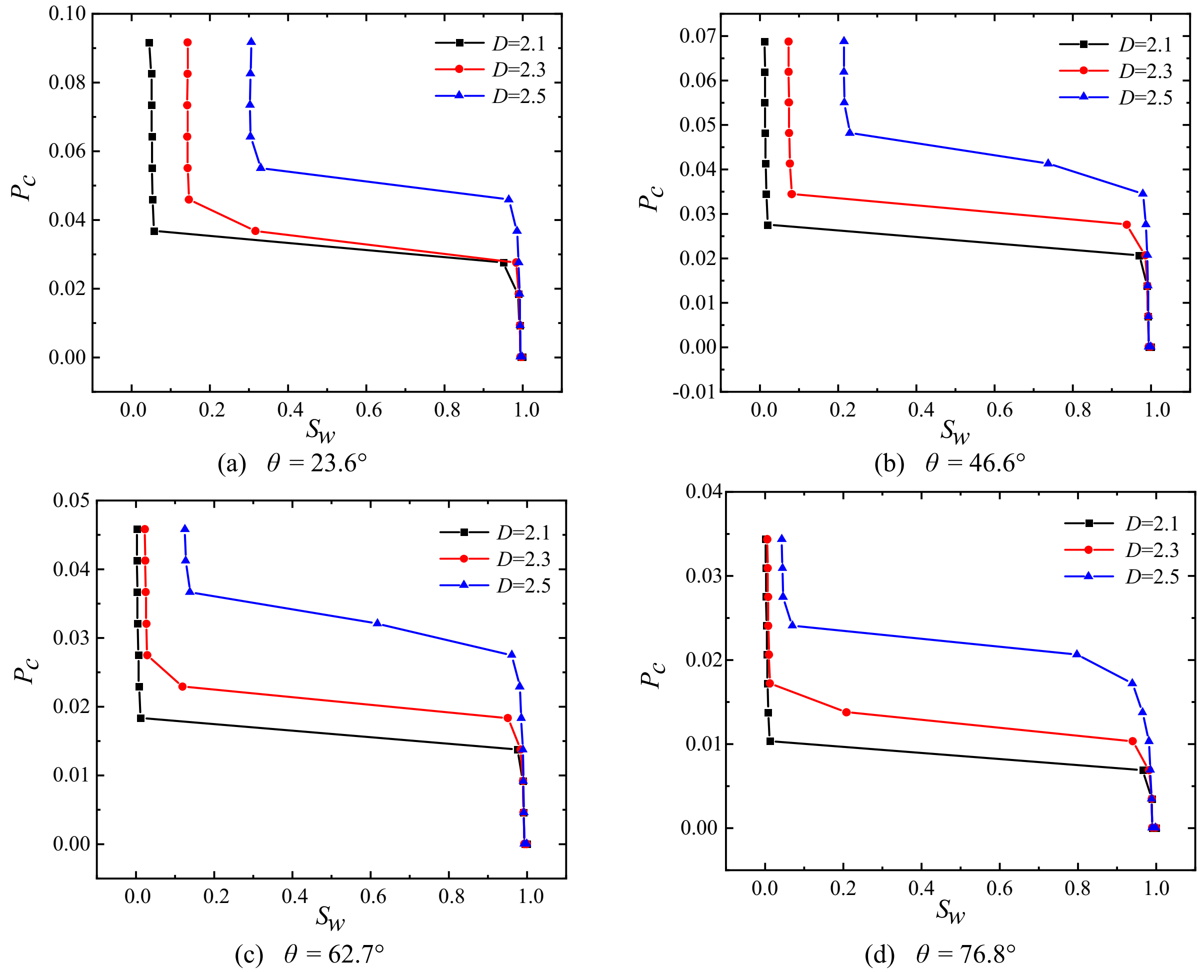

Fig. 9. Relationship between wetting-phase saturation and capillary pressure.

displacement flow properties through rough fractures. We used the successive random addition method to generate self-affine rough fracture surfaces with different roughness. Through duplicating and shifting operations on rough surfaces, we constructed matched fracture models with the same upper and lower surfaces and uniform aperture distribution. We employed the prevalent multicomponent Shan-Chen model in LBM to simulate a quasi-static drainage process under various wettabilities in three-dimensional rough-walled fractures. The simulation results demonstrated that greater roughness and stronger wettability of the fracture surface commonly destabilize the displacement process and make the invasion front more tortuous and irregular. Accordingly, there is a more visible remaining wetting phase near the outlet of fracture at breakthrough time.

In general, during the displacement process, the wetting phase saturation S_w gradually decreases with the advancement of invading front. Since the displacement fronts sometimes develop transversely and stop moving forward until they join other interfaces, a “step-like” type of S_w-X curve occurs, with the frontmost position almost unchanged while S_w sharply declines. The residual capture patterns are divided into two types: “isolated trapping” capture, where the wetting phase located in areas with drastic undulations of fracture surface is surrounded by the non-wetting phase, and “water film” capture, in which the wetting phase consistently adsorbs to the rough wall of fracture and is difficult to be displaced. Stronger wettability induces more captures of the second pattern due to the greater adsorption of wetting phase to the fracture wall. When P_c gradually increases to reach the entry pressure, S_w decreases rapidly and most of the wetting phases are completely expelled due to uniform aperture distribution, except for “water film” capture that is persistently adsorbed on the fracture wall. Therefore, continuously increasing P_c has no apparent effect on S_w variation once P_c is greater than the entry pressure P_e, and the first corner on the left side of P_c-S_w curves is relatively sharp. P_e increases with the improvement of fractal dimension and stronger wettability, which demonstrates that fractures with greater roughness and stronger wettability have larger displacement resistance in the invasion process, leading to more residual wetting phase saturation and lower displacement efficiency when the same P_c is applied.

Acknowledgements

We gratefully acknowledge the financial support from the National Natural Science Foundation of China (No. 42077243).

Conflict of interest

The authors declare no competing interest.

References

Al-Hashimi, O., Hashim, K., Loffill, E., et al. A comprehensive review for groundwater contamination and remediation: Occurrence, migration and adsorption modelling. Molecules, 2021, 26(19): 5913.

Al-Housseiny, T. T., Tsai, P. A., Stone, H. A. Control of interfacial instabilities using flow geometry. Nature Physics, 2012, 8(10): 747-750.

Babadagli, T., Raza, S., Ren, X., et al. Effect of surface roughness and lithology on the water-gas and water-oil relative permeability ratios of oil-wet single fractures. International Journal of Multiphase Flow, 2015a, 75: 68-81.

Babadagli, T., Ren, X., Develi, K. Effects of fractal surface roughness and lithology on single and multiphase flow in a single fracture: An experimental investigation. International Journal of Multiphase Flow, 2015b, 68: 40-58.

Bergslien, E., Fountain, J. The effect of changes in surface wettability on two-phase saturated flow in horizontal replicas of single natural fractures. Journal of Contaminant Hydrology, 2006, 88(3-4): 153-180.

Brown, S. R. Fluid flow through rock joints: The effect of surface roughness. Journal of Geophysical Research: Solid Earth, 1987, 92(B2): 1337-1347.

Cai, J., Chen, Y., Liu, Y., et al. Capillary imbibition and flow of wetting liquid in irregular capillaries: A 100-year review. Advances in Colloid and Interface Science, 2022, 304: 102654.

Cao, Y., Tang, M., Zhang, Q., et al. Dynamic capillary pressure analysis of tight sandstone based on digital rock model. Capillarity, 2020, 3(2): 28-35.

Chaaban, M., Heider, Y., Markert, B. Upscaling LBM-TPM simulation approach of Darcy and non-Darcy fluid flow in deformable, heterogeneous porous media. International Journal of Heat and Fluid Flow, 2020, 83: 108566.

Chang, C., Kneafsey, T. J., Wan, J., et al. Impacts of mixed-wettability on brine drainage and supercritical CO_2 storage efficiency in a 2.5-D heterogeneous micromodel. Water Resources Research, 2020, 56(7): e2019WR026789.

Charkaluk, E., Bigerelle, M., Iost, A. Fractals and fracture. Engineering Fracture Mechanics, 1998, 61(1): 119-139.

Chen, Y., Fang, S., Wu, D., et al. Visualizing and quantifying the crossover from capillary fingering to viscous fingering in a rough fracture. Water Resources Research, 2017, 53(9): 7756-7772.

Chen, Y. F., Wu, D. S., Fang, S., et al. Experimental study on two-phase flow in rough fracture: Phase diagram and localized flow channel. International Journal of Heat and Mass Transfer, 2018, 122: 1298-1307.

Dou, Z., Zhou, Z., Sleep, B. E. Influence of wettability on interfacial area during immiscible liquid invasion into a 3D self-affine rough fracture: Lattice Boltzmann simulations. Advances in Water Resources, 2013, 61: 1-11.

Glass, R. J., Nicholl, M. J., Yarrington, L. A modified invasion percolation model for low-capillary number immiscible displacements in horizontal rough-walled fractures: Influence of local in-plane curvature. Water Resources Research, 1998, 34(12): 3215-3234.

Guiltinan, E. J., Santos, J. E., Cardenas, M. B., et al. Two-phase fluid flow properties of rough fractures with heterogeneous wettability: Analysis with lattice Boltzmann simulations. Water Resources Research, 2021, 57(1): e2020WR027943.

Guo, R., Dalton, L., Crandall, D., et al. Role of heterogeneous surface wettability on dynamic immiscible displacement, capillary pressure, and relative permeability in a CO_2-water-rock system. Advances in Water Resources, 2022, 165: 104226.

Hao, L., Cheng, P. Lattice Boltzmann simulations of water transport in gas diffusion layer of a polymer electrolyte membrane fuel cell. Journal of Power Sources, 2010, 195(12): 3870-3881.

Holtzman, R., Segre, E. Wettability stabilizes fluid invasion into porous media via nonlocal, cooperative pore filling. Physical Review Letters, 2015, 115(16): 164501.

Hu, R., Zhou, C. X., Wu, D. S., et al. Roughness control on multiphase flow in rock fractures. Geophysical Research Letters, 2019, 46(21): 12002-12011.

Huang, H., Thorne, Jr. D. T., Schaap, M. G., et al. Proposed approximation for contact angles in Shan-and-Chen-type multicomponent multiphase lattice Boltzmann models. Physical Review E, 2007, 76(6): 066701.

Karpyn, Z. T., Grader, A. S., Halleck, P. M. Visualization of fluid occupancy in a rough fracture using micro-tomography. Journal of Colloid and Interface Science, 2007, 307(1): 181-187.

Landry, C. J., Karpyn, Z. T., Ayala, O. Relative permeability of homogenous-wet and mixed-wet porous media as determined by pore-scale lattice Boltzmann modeling. Water Resources Research, 2014, 50(5): 3672-3689.

Latt, J., Malaspinas, O., Kontaxakis, D., et al. Palabos: Parallel lattice Boltzmann solver. Computers & Mathematics with Applications, 2021, 81: 334-350.

Lenormand, R., Touboul, E., Zarcone, C. Numerical models and experiments on immiscible displacements in porous media. Journal of Fluid Mechanics, 1988, 189: 165-187.

Li, J., Li, X., Wu, K., et al. Thickness and stability of water film confined inside nanoslits and nanocapillaries of shale and clay. International Journal of Coal Geology, 2017, 179: 253-268.

Liu, H. H., Bodvarsson, G. S., Lu, S., et al. A corrected and generalized successive random additions algorithm for simulating fractional Levy motions. Mathematical

Geology, 2004, 36: 361-378.
Liu, Y., Berg, S., Ju, Y., et al. Systematic investigation of corner flow impact in forced imbibition. Water Resources Research, 2022, 58(10): e2022WR032402.
Liu, Y., Cai, J., Sahimi, M., et al. A study of the role of microfractures in counter-current spontaneous imbibition by lattice Boltzmann simulation. Transport in Porous Media, 2020, 133: 313-332.
Ma, G., Ma, C., Chen, Y. An investigation of nonlinear flow behaviour along rough-walled fractures considering the effects of fractal dimensions and contact areas. Journal of Natural Gas Science and Engineering, 2022, 104: 104675.
Meng, Q., Cai, J. Recent advances in spontaneous imbibition with different boundary conditions. Capillarity, 2018, 1(3): 19-26.
Neuweiler, I., Sorensen, I., Kinzelbach, W. Experimental and theoretical investigations of drainage in horizontal rough-walled fractures with different correlation structures. Advances in Water Resources, 2004, 27(12): 1217-1231.
Pruess, K., Tsang, Y. W. On two-phase relative permeability and capillary pressure of rough-walled rock fractures. Water Resources Research, 1990, 26(9): 1915-1926.
Qiu, Y., Xu, K., Pahlavan, A. A., et al. Wetting transition and fluid trapping in a microfluidic fracture. Proceedings of the National Academy of Sciences of the United States of America, 2023, 120(22): e2303515120.
Santos, J. E., Gigliotti, A., Bihani, A., et al. MPLBM-UT: Multiphase LBM library for permeable media analysis. SoftwareX, 2022, 18: 101097.
Shan, B., Wang, P., Wang, R., et al. Molecular kinetic modelling of nanoscale slip flow using a continuum approach. Journal of Fluid Mechanics, 2022, 939: A9.
Shan, X., Chen, H. Lattice Boltzmann model for simulating flows with multiple phases and components. Physical review E, 1993, 47(3): 1815-1819.
Sheng, J., Huang, T., Ye, Z., et al. Evaluation of van Genuchten-Mualem model on the relative permeability for unsaturated flow in aperture-based fractures. Journal of Hydrology, 2019, 576: 315-324.
Tang, M., Zhan, H., Ma, H., et al. Upscaling of dynamic capillary pressure of two-phase flow in sandstone. Water Resources Research, 2019, 55(1): 426-443.
Trojer, M., Szulczewski, M. L., Juanes, R. Stabilizing fluid-fluid displacements in porous media through wettability alteration. Physical Review Applied, 2015, 3(5): 054008.
Wang, H., Cai, J., Su, Y., et al. Imbibition behaviors in shale nanoporous media from pore-scale perspectives. Capillarity, 2023, 9(2): 32-44.
Wang, H., Yuan, X., Liang, H., et al. A brief review of the phase-field-based lattice Boltzmann method for multiphase flows. Capillarity, 2019, 2(3): 33-52.
Wang, L., Cardenas, M. B. Connecting pressure-saturation and relative permeability models to fracture properties: The case of capillary-dominated flow of supercritical CO_2 and brine. Water Resources Research, 2018, 54(9): 6965-6982.
Yamabe, H., Tsuji, T., Liang, Y., et al. Lattice Boltzmann simulations of supercritical CO_2-water drainage displacement in porous media: CO_2 saturation and displacement mechanism. Environmental Science & Technology, 2015, 49(1): 537-543.
Yang, Z., Li, D., Xue, S., et al. Effect of aperture field anisotropy on two-phase flow in rough fractures. Advances in Water Resources, 2019, 132: 103390.
Yao, C., Shao, Y., Yang, J., et al. Effects of non-darcy flow on heat-flow coupling process in complex fractured rock masses. Journal of Natural Gas Science and Engineering, 2020, 83: 103536.
Ye, Z., Fan, X., Zhang, J., et al. Evaluation of connectivity characteristics on the permeability of two-dimensional fracture networks using geological entropy. Water Resources Research, 2021, 57(10): e2020WR029289.
Ye, Z., Liu, H. H., Jiang, Q., et al. Two-phase flow properties of a horizontal fracture: The effect of aperture distribution. Advances in Water Resources, 2015, 76: 43-54.
Ye, Z., Liu, H. H., Jiang, Q., et al. Two-phase flow properties in aperture-based fractures under normal deformation conditions: Analytical approach and numerical simulation. Journal of Hydrology, 2017, 545: 72-87.
Ye, Z., Yang, J. Experimental study of real-time temperature-dependent nonlinear deformation of sandstone. Fuel, 2023, 354: 129308.
Yi, J., Liu, L., Xia, Z., et al. Effects of wettability on relative permeability of rough-walled fracture at pore-scale: A lattice Boltzmann analysis. Applied Thermal Engineering, 2021, 194: 117100.
Zhang, T., Javadpour, F., Li, J., et al. Pore-scale perspective of gas/water two-phase flow in shale. SPE Journal, 2021, 26(2): 828-846.
Zhao, B., MacMinn, C. W., Juanes, R. Wettability control on multiphase flow in patterned microfluidics. Proceedings of the National Academy of Sciences of the United States of America, 2016, 113(37): 10251-10256.
Zhao, J., Kang, Q., Yao, J., et al. The effect of wettability heterogeneity on relative permeability of two-phase flow in porous media: A lattice Boltzmann study. Water Resources Research, 2018, 54(2): 1295-1311.
Zhou, Y., Guan, W., Zhao, C., et al. Spontaneous imbibition behavior in porous media with various hydraulic fracture propagations: A pore-scale perspective. Advances in Geo-Energy Research, 2023, 9(3): 185-197.
Zou, Q., He, X. On pressure and velocity boundary conditions for the lattice Boltzmann BGK model. Physics of Fluids, 1997, 9(6): 1591-1598.